Segmentation of tumor necrosis by mapping fractional plasma volume (fPV) from dynamic albumin-(Gd-DTPA)30 enhanced MRI for evaluation of therapeutic response to gefitinib in breast cancer model

K-L. Li[1], L. Wilmes[1], S. Aliu[1], D. Wang[2], B. HANN[2], M. Moasser[3], and N. Hylton[1]

[1]Radiology, University of California, San Francisco, San Francisco, CA, United States, [2]Comprehensive Cancer Center, University of California, San Francisco, San Francisco, CA, United States, [3]Medicine, University of California, San Francisco, San Francisco, CA, United States

INTRODUCTION

It has been recommended that, for appropriate assessment of tumor response to therapeutics using dynamic contrast agent enhanced (DCE) MRI, areas of necrosis, adjacent blood vessels and artefacts should be excluded (1). Generally ROIs are manually tracked to cover the tumor rim and the tumor core. This approach, however, does not account for the considerable microcirculatory heterogeneity within the tumor. Another way of excluding necrotic regions is by setting voxel inclusion criteria on a pixel-by-pixel basis. In the current DCE-MRI study with albumin-(Gd-DTPA)$_{30}$, we introduced a method of segmenting tumor necrosis based on the hypothesis that regions with undetectable vascular volume on maps of fractional plasma volume (fPV) may reflect the extent of tumor necrosis. The purpose of this study is to explore the feasibility of using this segmentation method in albumin-(Gd-DTPA)$_{30}$ enhanced MRI. A computer simulation is used for validation. A mouse model of breast cancer is used to estimate tumor response to treatment of gefitinib (ZD1839), an epidermal growth factor receptor (EGFR) tyrosine kinase inhibitor.

METHODS

Kinetic Model and Computer Simulation: A two-compartment, unidirectional pharmacokinetic model (Patlak model) was used in the simulation and experimental data analysis (Eq. 1). The reliability of using fPV maps for segmenting tumor necrotic area was examined by computer simulation. An array (128x128) of theoretical tissue uptake curves was simulated based on Eq. 1 for K_{ps} ranging from 0.0 to 0.2 ml/(min·100ml) and fPV ranging from 0.0 to 0.1, and were used to construct the synthetic dynamic signal intensity curves. Zero-mean Gaussian noise was added to generate synthetic data sets with a signal to noise ratio of 20. The synthetic data sets were then analyzed with the Patlak model. Goodness-of-fit was estimated by scaled fitting errors (Eq. 2), where A and T are experimental and theoretical data respectively (2). Unfitted voxels (SFE > 50%) and voxels with the fitted fPV ≤ 0 were taken as the necrotic area (set to fPV=0.0) and compared with the 'true' fPV data to evaluate the reliability of the segmentation.

$$C_t(t) = fPV \cdot C_p(t) + K^{ps} \cdot \int_0^t C_p(t')dt' \quad [1]$$

$$SFE = \sqrt{\frac{\sum_i (T_i - A_i)^2}{\sum_i A_i^2}} \times 100\% \quad [2]$$

Animal Study: Female nude mice were implanted subcutaneously in the axial flank with the human breast cancer line BT474, a Her2/neu over-expressing variant. Gefitinib was administerd as a 2-day (1000 mg/kg per day) pulse. DCE-MRI was performed before and on the first and fifth day after the treatment. Lesion boundaries were assigned manually in the DCE MRI images. The values of K^{ps}, fPV and SFE were estimated on a pixel-by-pixel basis for the ROIs encompassing the entire tumor. The numbers of voxels within the whole tumor volume and within the perfused tumor tissue area (SFE ≤ 50% and 0 < fPV < 0.5) were counted for each tumor before and after the treatment. The median, mean, and SD for fPV or K^{ps} within the perfused tumor tissue area were estimated for each tumor at each MRI exams. Group fractional histograms of fPV or K^{ps} before and after treatment were generated by pooling together all perfused voxels in the tumors of each group and then normalizing by the total number of the perfused tumor voxels in the group. The group-averaged SI enhancement curves of the perfused tumor tissue area and the necrotic area were also calculated and compared.

RESULTS

Simulation: Fig. 1 demonstrates the fPV maps of 'true' values (a) and the fitted values (b). The pixel-by-pixel difference between the 'true' and fitted fPV was -0.0002±0.003. The voxels with undetectable fPV (black area in Fig. 1b) are around the area with 'true' fPV < 0.004 and K^{ps} < 0.06 ml/(min·100ml).

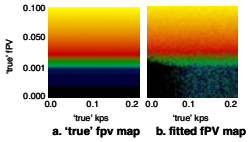

Fig. 1. Computer simulated fPV maps.

Animal Study: Fig. 2 shows the total tumor volume and the fractional tumor volume with detectable fPV before and after the pulse gefitinib treatment. The latter shows a statistically significant decrease on the 1st day after the 2-day pulse dosing. Fig.3 shows the fPV group fractional histograms for the treated groups before (black), and on the 1st day (red) and 5th day (green) after the 2-day pulse dosing. The group averaged median, mean and SD values of fPV in the perfused tumor tissue area (fig. 3) showed a transient increase on the 1st day after the pulse dosing, and returned to pretreatment values by the 5th day. Fig.4 shows the K^{ps} group fractional histograms for the treated groups before (black), and on the 1st day (red) and 5th day (green) after the 2-day pulse gefitinib treatment, and the group averaged median, mean and SD values of K^{ps} in the perfused tumor tissue area. The tumor K^{ps} showed a transient decrease in the median and mean values on the 1st day after the pulse dosing, and an increase on the 5th day, but a transient increase in the SD value on the 1st day after the pulse dosing, and a decrease on the 5th day. It is interesting to see that the number of voxels, which appeared with negative K^{ps} values, had a transient increase on the 1st day after the pulse dosing, and then decreased by the 5th day. Fig. 5 shows the group-averaged SI enhancement curves for the necrotic area (black), the perfused tumor tissue area with $K^{ps} \geq 0$ (red) and $K^{ps} < 0$ (green) from the exam on the 1st day after pulse dosing. The MRI signal intensity (SI) curve from the necrosis area shows little change after the injection. The MRI SI from the perfused tumor tissue area with K^{ps} < 0 showed a higher pre-contrast intensity than the positive K^{ps} area, and started a fast decay around 3 minutes after the injection, which is clearly distinguishable from the 'normal' enhancement curve (red).

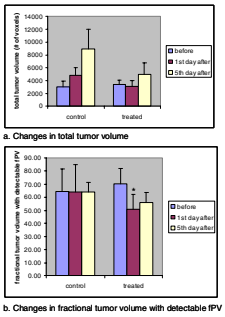

Fig. 2. Changes in tumor volume.

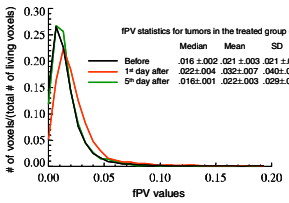

Fig. 3. fPV group fractional histograms

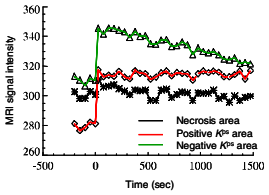

Fig. 5. Three types of SI vs time curves

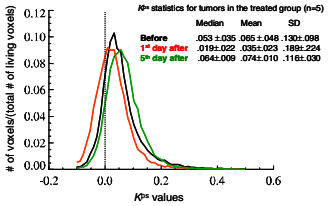

Fig. 4. K^{ps} group fractional histograms

DISCUSSION

The analysis of fPV distribution in the whole mass of tumor allowed the quantification of the extent of the necrotic tumoral core. In addition, the perfused tumor tissues were further divided into the extravascular *pooling* (positive K^{ps}, i.e., voxels in which the contrast agent accumulated over time) and *draining* (negative K^{ps}, i.e., voxels from which the contrast agent was eliminated over time) voxels (3), based on K^{ps} maps calculated from dynamic albumin-(Gd-DTPA)$_{30}$ enhanced MRI using an unidirectional two-compartment model. Having applied these methods to evaluate the response of the experimental breast cancer model to pulse dosing of gefitinib, we found: (1) a decrease in the fractional tumor volume with detectable fPV after the 2-day pulse gefitinib treatment; (2) a transient increase in mean fPV observed on the 1st day after the pulse dosing of gefitinib, which may be related to hemodynamic dilation of the remaining vessels; (3) a transient decrease in mean K^{ps}, accompanied by a transient increase in the number of the extravascular *draining* voxels observed on the 1st day after the pulse dosing of gefitinib. The drainage of macromolecules contrast agent in viable regions of tumors occurs either by convection and/or tumoral lymphatics, if present. These findings may help in probing the remodeling of the extravascular space in tumors that often accompanies therapeutic interventions, and improving the delivery and transport of anticancer drugs.

References: [1] Leach et al. Br J Radiol 2003;76 Suppl 1:S87-91. [2] Li et al. Br J Radiol 2000;73(869):470-481. [3] Pathak et al. Cancer Res 2005;65(4):1425-1432.

Acknowlegements: NIH 2ROICA69587